

Design of a tunable Airy zoom metasurface based on the moiré effect

Baibing Li(李白冰), Jiatong Liu(刘家同), Hao Huang(黄浩), and Ruiting Hao(郝瑞亭)

Citation: Chin. Phys. B, 2026, 35 (**6**): 064211. DOI: 10.1088/1674-1056/ae5592
http://cpb.iphy.ac.cn; http://iopscience.iop.org/cpb

What follows is a list of articles you may be interested in

Continuous three-dimensional varifocal of vortex beams with twisted metasurfaces

Yiyi Li(黎仪艺), Wangzhe Zhou(周王哲), Shaoqi Li(李少奇), Xiaoyan Huang(黄晓艳), Fen Zhao(赵芬), Man Yuan(袁满), Jiagui Wu(吴加贵), Huan Chen(陈欢), Zhaojian Zhang(张兆健), and Junbo Yang (杨俊波)
Chin. Phys. B, 2026, 35 (**3**): 034208. DOI: 10.1088/1674-1056/adfc42

Room-temperature exciton-polariton condensation in pressed perovskite microcavities

Tianyin Zhu(朱天寅), Zelei Chen(陈泽磊), Xiaoyu Wang(王小宇), Zhongmin Huang(黄钟民), Haibin Zhao(赵海斌), and Jun Wang(王俊)
Chin. Phys. B, 2025, 34 (**9**): 094202. DOI: 10.1088/1674-1056/addce6

Dynamic and polarization-independent high-*Q* guided resonances in metasurfaces with phase change material

Guozhong Zhang(张国忠), Mimi Zhou(周秘密), Hong Xiang(向红), and Dezhuan Han(韩德专)
Chin. Phys. B, 2025, 34 (**8**): 084201. DOI: 10.1088/1674-1056/add1bb

All-chalcogenide glass based high fill-factor long-wave infrared micro-metalens array with superior optical flexibility

Zhaofeng Gu(谷招峰), Kongsi Zhou(周孔思), Tong Sun(孙童), Yixiao Gao(高一骁), Yimin Chen(陈益敏), Zijun Liu(刘自军), Chenjie Gu(顾辰杰), Pengfei Lu(芦鹏飞), and Xiang Shen(沈祥)
Chin. Phys. B, 2025, 34 (**7**): 074213. DOI: 10.1088/1674-1056/add4f5

Effective working regions of the grating chip for planar-integrated magneto-optics trap

Chang-Jiang Huang(黄长江), Ling-Xiao Wang(王凌潇), Liang Chen(陈梁), Chuan-Feng Li(李传锋), Guang-Can Guo(郭光灿), Chang-Ling Zou(邹长铃), and Guo-Yong Xiang(项国勇)
Chin. Phys. B, 2025, 34 (**7**): 074211. DOI: 10.1088/1674-1056/adcb9c

---

Design of a tunable Airy zoom metasurface based on the moiré effect

Baibing Li(李白冰)[1], Jiatong Liu(刘家同)[2], Hao Huang(黄浩)[1,†], and Ruiting Hao(郝瑞亭)[2,‡]

[1] *Guangxi Key Laboratory of Processing for Non-Ferrous Metals and Featured Materials, School of Resources, Environment and Materials, Guangxi University, Nanning* 530004, *China*

[2] *College of Energy and Environment Science, Yunnan Normal University, Kunming* 650500, *China*

(Received 4 January 2026; revised manuscript received 10 March 2026; accepted manuscript online 23 March 2026)

Dynamic control of Airy beam focusing is important for applications in optical manipulation, imaging, and laser processing. However, most metasurface-based Airy beam generators are statically designed, and tunability typically relies on mechanical translation, which limits system compactness and integration. Here, we propose a tunable Airy zoom metasurface based on the moiré effect. The device consists of two rotationally symmetric dielectric metasurfaces composed of titanium dioxide nanopillars. By encoding the Airy autofocusing phase and exploiting the rotational moiré modulation between the two layers, the output phase distribution can be continuously tuned through relative rotation, enabling dynamic control of the Airy beam focal position. Numerical simulations demonstrate that at a wavelength of 610 nm the focal length can be continuously tuned from 8 μm to 32 μm. Compared with conventional quadratic-phase moiré zoom metasurfaces, the proposed design preserves the nondiffracting characteristics of Airy beams while providing improved focusing efficiency and enhanced lateral resolution. This work offers a compact and mechanically simple approach for dynamically controllable metasurface optics and may facilitate the development of integrated and programmable photonic systems.

Keywords: metasurface, airy beam, autofocus

PACS: 42.79.Bh, 42.25.Fx, 78.67.Pt

DOI: 10.1088/1674-1056/ae5592 **CSTR:** 32038.14.CPB.ae5592

1. Introduction

In 2010, Efremidis *et al*. proposed, from a mathematical perspective, a novel method for generating a new type of abruptly autofocusing beam.[1] Such beams are capable of exhibiting sudden focusing at a predesigned focal position, accompanied by a pronounced enhancement of optical energy. These beams are typically realized by constructing a radially symmetric configuration through revolving a one-dimensional Airy beam around the optical axis, or alternatively by appropriately superposing arrays of Airy wave packets, thereby exhibiting characteristic autofocusing behavior.[2] Consequently, if Airy autofocusing beams — combining self-healing and diffraction-free properties — can be further endowed with dynamic tunability, they are expected to demonstrate significantly enhanced potential in applications such as imaging and sensing. However, in conventional optical systems, tunability is usually achieved through the coordinated operation of multiple optical elements and complex adjustment strategies, which severely limits system integration and stability. In recent years, metasurfaces have developed rapidly in areas such as planar optics, ultrathin lenses, and lightweight optical devices, becoming a major frontier in optical research.[3–6] Owing to their advantages of low weight, low cost, and the ability to eliminate spherical aberrations,[7–10] metalenses have demonstrated great potential in applications including imaging, spectroscopy, lithography, and laser processing.[11–23] Among these, mechanically tunable varifocal metalenses have attracted significant attention. Colburn *et al*. designed an optical system composed of two metasurfaces based on the Alvarez lens principle, in which the focal length of the outgoing beam can be tuned by adjusting the lateral displacement between the two metasurfaces; the maximum zoom range is determined by the maximum achievable lateral offset.[24] In 2019, Wei *et al*. combined metalens design with the zooming principle of moiré lenses and proposed a high-magnification rotational varifocal metalens operating at a wavelength of 1550 nm.[25] Compared with conventional zoom systems, this structure enables, in theory, an infinite zoom ratio through relative rotation rather than by changing the spacing between optical elements, thereby offering higher integration and stronger zooming capability. However, such structures do not possess diffraction-free characteristics or self-healing properties.

We show that the moiré effect's rotational tuning capability can be mathematically unified with the Airy beam. By encoding the Airy phase into the mutual rotation framework, it is possible to create a device that combines the 'zoom' of moiré lenses with the 'non-diffracting' nature of Airy beams. In response to the above issues, this paper proposes a tunable Airy zoom metasurface design method based on the moiré effect. By combining the moiré effect with the Airy autofocusing phase, continuous focal length tuning from 8 μm to 32 μm

†Corresponding author. E-mail: hhuang@gxu.edu.cn

‡Corresponding author. E-mail: ruitinghao@ynnu.edu.cn

© 2026 Chinese Physical Society and IOP Publishing Ltd. All rights, including for text and data mining, AI training, and similar technologies, are reserved.

at a wavelength of 610 nm is achieved solely by adjusting the relative rotational angle between the structures, without changing the inter-device spacing. Compared with conventional pure moiré zoom lenses,[25] the proposed approach not only inherits the diffraction-free and self-healing properties of Airy beams, but also exhibits further improvements in resolution and optical efficiency.

2. Design methodology

To achieve continuously tunable focal control while preserving the autofocusing propagation characteristics of Airy beams, a phase modulation strategy capable of flexibly reconfiguring the wavefront within a planar optical architecture is required. Leveraging the rotational zooming properties of moiré metasurfaces, we construct a bilayer cascaded phase modulation scheme in which the synthesized phase distribution can be continuously evolved through relative rotation between the two metasurface layers. By incorporating the Airy autofocusing phase into this rotational moiré phase synthesis framework, the proposed approach enables dynamic tuning of the Airy beam focal position without mechanical translation or variation of the interlayer spacing, while maintaining the diffraction-free and self-healing propagation properties of Airy beams.

A tunable Airy zoom metasurface refers to a device formed by combining two circular metasurfaces with zoom-phase profiles. By rotating the two metasurfaces relative to each other, the synthesized output phase can be modified, thereby tuning the focal length of the generated self-focusing Airy beam, as illustrated in Fig. 1.

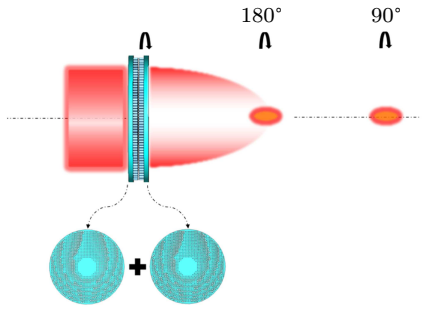


Fig. 1. Schematic diagram of the metasurface.

The designed metasurface in this work consists of rotationally symmetric cylindrical dielectric nanopillars. Its phase modulation relies on the propagation phase mechanism and exhibits polarization-independent characteristics. Therefore, to match the ideal phase distribution obtained from theoretical calculations, it is necessary to construct a phase database of nanopillars. We employed the commercial software "FDTD Solutions" (from ANSYS) to perform finite-difference time-domain (FDTD) simulations of the nanopillars. By incrementing each geometric parameter with a step size of 2 nm, the phase variation data of the nanopillars were acquired. Periodic boundary conditions were set in the x and y directions, while perfectly matched layer (PML) boundary conditions were applied in the z direction. The height of the nanopillars was fixed at 600 nm, with the diameter scanning range set from 100 nm to 300 nm, and the period of the nanopillar array was fixed at 320 nm. As shown in Fig. 2(a), when the period is 320 nm, the obtained transmission phase database fully covers the required phase distribution range, meeting the phase-matching design requirements.

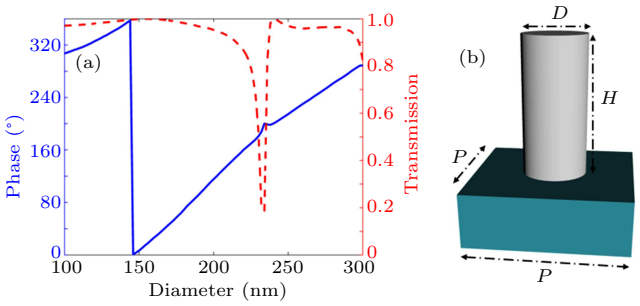


Fig. 2. (a) The phase and transmittance distributions of the unit cell structure (b) at a wavelength of 610 nm when the period P is 320 nm. (b) Schematic diagram of the unit cell structure, where the substrate material is silica, the unit cell material is titanium dioxide, the height H is 600 nm, and the period P is 320 nm.

Design the theoretical phase distribution of two metasurface layers by combining the moiré effect with the Airy autofocusing phase.

$$\varphi_1(r_0,\theta) = \frac{8}{3\lambda} a^{\frac{1}{2}} (r_0 - b)^{\frac{3}{2}} \phi(r_0), \tag{1}$$

$$\varphi_2(r_0,\theta) = -\frac{8}{3\lambda} a^{\frac{1}{2}} (r_0 - b)^{\frac{3}{2}} (\phi(r_0) + \theta), \tag{2}$$

$$\varphi(r_0,\theta) = \varphi_1(r_0,\theta) + \varphi_2(r_0,\theta) = -\frac{8}{3\lambda} a^{\frac{1}{2}} (r_0 - b)^{\frac{3}{2}} \theta. \tag{3}$$

Physically, the working principle can be understood as follows: the phase profile of each individual metasurface layer contains a specific spiral phase component. When the two layers overlap with a relative rotation angle θ, the cross-term in the superimposed phase creates a radial quadratic phase term (r^2). This induced quadratic term acts as an equivalent variable lens, where the optical power (the inverse of the focal length) is directly proportional to the rotation angle θ. By integrating the Airy beam's cubic phase modulation into this variable lens framework, the system achieves dynamic focal shifting while maintaining the characteristic non-diffracting propagation of Airy beams.

Here θ represents the relative rotation angle between the two metasurfaces, which can be expressed as $\theta = \pi/t$; the parameter t is introduced to facilitate the subsequent derivation of the focal length. It is defined as the ratio of the rotation angle to π, serving solely as a mathematical simplification and carrying no physical significance; r_0 denotes the radial size of the metasurface, and b indicates the inner radius size of the

metasurface annular region; ϕ denotes the relative rotation angle of the structure.

And the Airy autofocusing phase can be expressed as[26,27]

$$\varphi_{\text{airy}}(r_0) = -\frac{8\pi}{3\lambda} a^{\frac{1}{2}} (r_0 - b)^{\frac{3}{2}}. \tag{4}$$

The corresponding focal length is $f_o = \sqrt{b/a}$. Comparing formulas (3) and (4), it can be concluded that the focal length corresponding to formula (3) is $f = t \times f_o$.

After simplification and derivation, we obtain a phase formula in which the focal length can be continuously varied with the rotation angle.

The ideal phase profile is matched against the phase database (derived from the transmission phase library) to identify the corresponding unit structures, thereby completing the full modeling of the metasurface.

3. Results and discussion

This paper employs a 610 nm wavelength plane wave as the incident light, with a metasurface aperture of 8 μm. Full-wave FDTD simulations adopt perfectly matched layer (PML) boundary conditions in the X, Y, and Z directions, with a grid resolution set to 0.25 nm. The simulation region is defined as X direction (−9 μm to 9 μm), Y direction (−9 μm to 9 μm), .

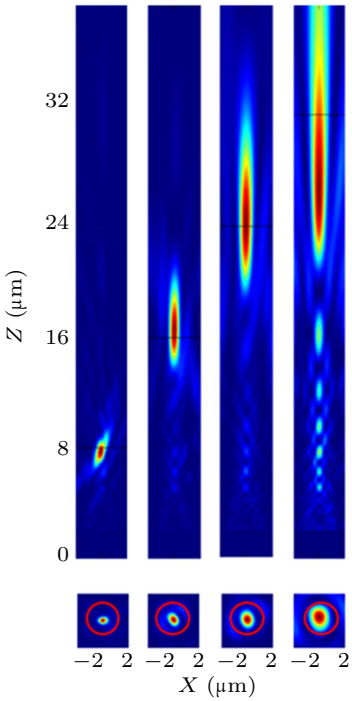


Fig. 3. Simulated lateral optical intensity distributions of the tunable Airy zoom metasurface without phase rounding quantization. From left to right, the columns correspond to relative rotation angles of π, $\pi/2$, $\pi/3$, and $\pi/4$, targeting theoretical focal lengths of 8 μm, 16 μm, 24 μm, and 32 μm, respectively. The red dashed boxes highlight significant spot distortions and severe aberrations caused by the sectorial effect inherent in the moiré rotation, which degrades the beam quality before optimization.

and Z direction (−0.3 μm to 1.5 μm). The far-field distribution is obtained using the farfieldexact3d function within the FDTD script. The material data for titanium dioxide (TiO_2) is sourced from Ref. [28]. In Eq. (3), parameter a is set to 31250 and parameter b to 2 μm, in order to make f_o equal to 8 μm.

The relative rotation angles between the two metasurface layers are set to π, $\pi/2$, $\pi/3$, and $\pi/4$, corresponding to theoretical focal lengths of 8 μm, 16 μm, 24 μm, and 32 μm, respectively. The simulation results are shown in Fig. 3.

The ideal Airy disk should be a symmetric circle. However, the lateral light field distribution in Fig. 3 (specifically, the region highlighted in red) reveals significant spot deformation compared to a standard circle, indicating the presence of severe aberration. This distortion stems primarily from the sectorial effect generated during the rotation of the moiré pattern.[29] To mitigate this issue in the phase processing stage, we introduced the round function for phase quantization. The corresponding simulation results after quantization are presented in Fig. 4.

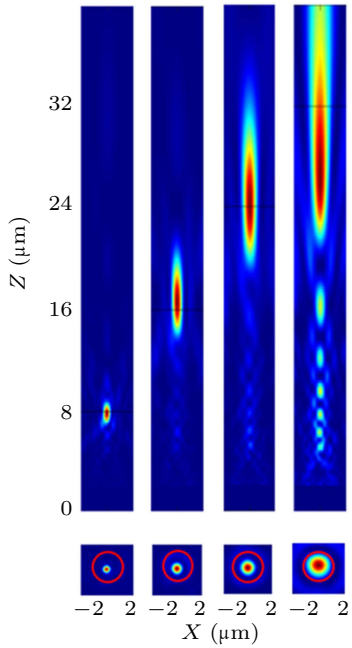


Fig. 4. Optimized lateral optical intensity distributions after applying the phase rounding function. From left to right, the columns correspond to relative rotation angles of π, $\pi/2$, $\pi/3$, and $\pi/4$, targeting theoretical focal lengths of 8 μm, 16 μm, 24 μm, and 32 μm, respectively. Compared to Fig. 3, the focal spots exhibit significantly improved circular symmetry and reduced side-lobes. This demonstrates that the rounding operation effectively suppresses the sectorial aberration, preserving the quality of the Airy beam across the entire tuning range.

By comparing Figs. 3 and 4, it can be observed that the optical field results presented in Fig. 4 are significantly improved after the rounding operation compared to those in Fig. 3. The aberration correction is significantly improved, which demonstrates that the designed Airy zoom metasurface can still effectively achieve focusing even when the focal length changes. This leads to an important question worthy

of further exploration: once the relationship between the focal length and rotation angle is established, the selection of parameters a and b and their influence on the focused optical field constitute a valuable research topic.

When the base focal length f_o (at rotation angle π) is fixed, according to $f_o = \sqrt{b/a}$, a is a quantity that varies with b. Here, b represents the inner radius of the hollow annular metasurface, and since the outer radius R (i.e., the aperture) of the metasurface is fixed, we use a ratio parameter ε ($\varepsilon = b/R$) to represent the variation of b.

We set ε to two extreme and visually contrasting values of 0.05 and 0.8, with the simulation results shown in Fig. 5 below.

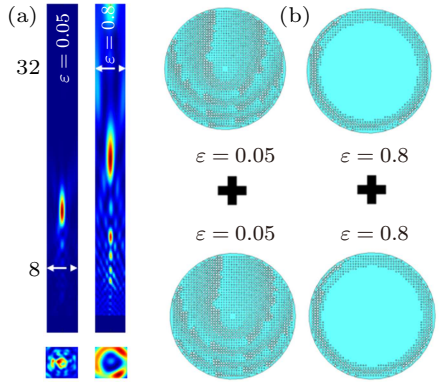


Fig. 5. Influence of the inner-to-outer radius ratio $\varepsilon = b/R$ on focusing behavior. (a) Left: field distribution for $\varepsilon = 0.05$ at $\theta = \pi$ (designed focus 8 μm); right: field distribution for $\varepsilon = 0.8$ at $\theta = \pi/4$ (designed focus 32 μm). (b) Corresponding metasurface layouts (top view) for $\varepsilon = 0.05$ (left) and $\varepsilon = 0.8$ (right). Small ε leads to delayed focusing, while large ε causes early focusing, consistent with the curved trajectory of Airy beams.

As shown in Fig. 5, when ε is small, the metasurface may exhibit delayed focusing, whereas when ε is large, the opposite effect occurs. This is primarily because Airy beams propagate along curved trajectories, and the curvature of the trajectory is closely related to ε[27] ($r(z) = b - az^2$), as illustrated in Fig. 6.

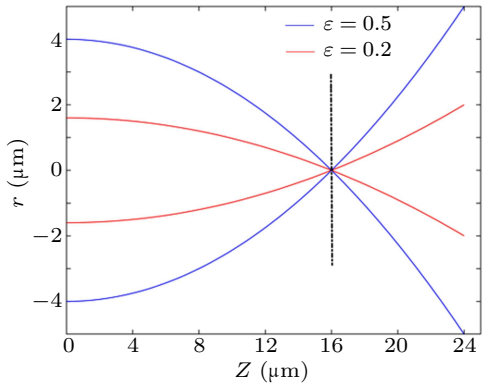


Fig. 6. Geometry of the autofocusing beam.

From Fig. 6, it can be seen that when the ideal focal length is 16 μm and ε is 0.2, the orbital curvature is significantly smaller than when ε is 0.5. This can lead to issues such as an extended depth of focus and a backward shift of the focal point, particularly when the focal length is small relative to the lens aperture and ε is also small. In such cases, the problem becomes more pronounced. Conversely, when ε is large, a situation similar to that shown in the right panel of Fig. 5(a) may occur.

Therefore, we can roughly summarize a rule: when the overall numerical aperture of the metasurface is large, choosing a smaller ε is more appropriate; whereas when the numerical aperture is small, selecting a larger ε is more suitable.

On the other hand, there have also been reports[25] on calculating the phase of moiré zoom metasurfaces based on the following equations:

$$\varphi_1(r,\theta) = \text{round}\left[\frac{1}{\lambda \cdot f_0} r^2\right] \phi(r), \tag{5}$$

$$\varphi_2(r,\theta) = -\text{round}\left[\frac{1}{\lambda \cdot f_0} r^2\right] (\phi(r) + \theta), \tag{6}$$

$$\varphi = \varphi_1(r,\theta) + \varphi_2(r,\theta) = -\text{round}\left[\frac{1}{\lambda \cdot f_0} r^2\right] \theta. \tag{7}$$

By comparing Eq. (7) with the quadratic phase, it can be derived that the focal length of the metasurface follows the relationship $f = \frac{\pi}{\theta} f_o$ with the rotation angle, which is consistent with the relationship between focal length and rotation angle presented in this paper.

Under the same conditions, the calculation results of this metasurface are shown in Fig. 7.

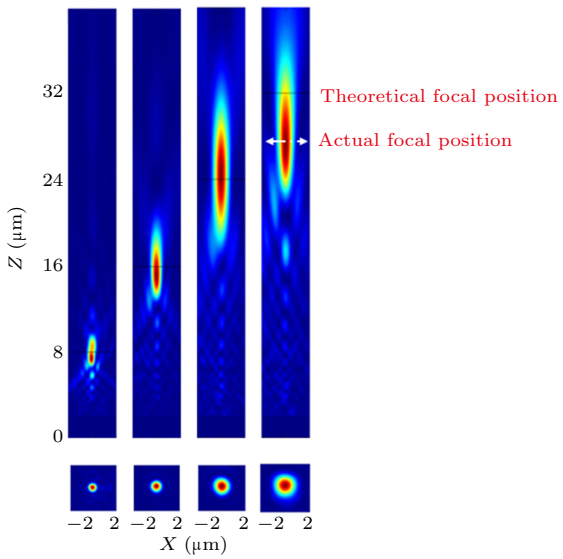


Fig. 7. Simulated field distribution of the quadratic-phase moiré zoom metasurface (without Airy phase). From left to right, the columns correspond to relative rotation angles of π, $\pi/2$, $\pi/3$, and $\pi/4$, targeting theoretical focal lengths of 8 μm, 16 μm, 24 μm, and 32 μm, respectively. Notably, at the rotation angle of $\pi/4$ (rightmost column, target $f = 32$ μm), the focal spot shows severe energy dispersion and defocusing compared to the Airy design in Fig. 4. This verifies that the quadratic-phase design suffers from significant longitudinal aberration at large zoom ranges, whereas the proposed Airy design maintains a tighter focus.

As can be seen from Fig. 7, when the rotation angle is 0.25π, the metasurface exhibits severe defocusing. When the rotation angle is π, the depth of focus increases and the energy

distribution becomes uneven. This is primarily due to the limitations of the paraxial approximation inherent in the quadratic phase itself.

The full width at half maximum (FWHM) and focusing efficiency of this metasurface are compared with those of the $\varepsilon = 0.25$ Airy zoom metasurface mentioned earlier, as shown in Fig. 8 and Table 1.

Based on the observation of Fig. 8 and Table 1, except at the 32 μm focal position where the quadratic-phase metasurface exhibits a larger FWHM, degraded resolution, and an artificially high energy reading due to defocusing, the Airy zoom metasurface demonstrates superior performance in both efficiency and resolution across the remaining focal lengths. This indicates a more concentrated energy convergence in the proposed design.

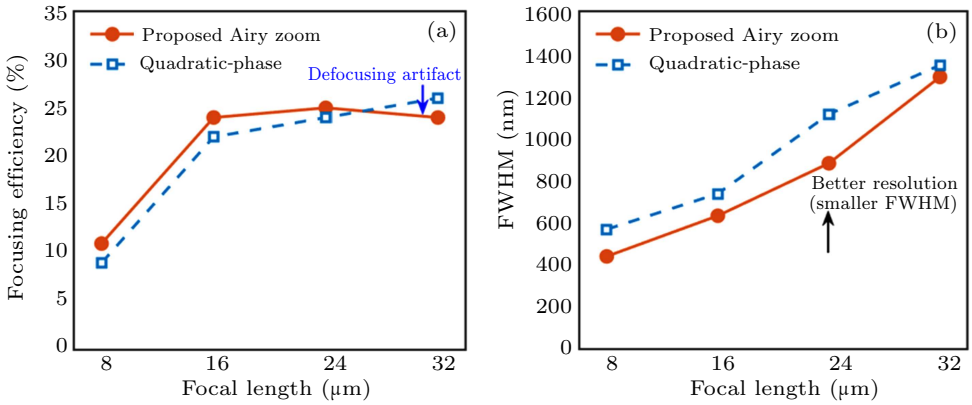


Fig. 8. Quantitative performance comparison between the proposed Airy zoom metasurface and the conventional quadratic-phase zoom metasurface. (a) Focusing efficiency across different focal lengths. The proposed design demonstrates higher efficiency for most focal lengths. Note that the slightly higher efficiency of the quadratic lens at 32 μm is an artifact caused by beam defocusing, which spreads energy axially rather than confining it to the focal spot. (b) FWHM of the focal spots. The proposed Airy design consistently achieves smaller FWHM values (better resolution) compared to the quadratic design, with an average resolution enhancement of approximately 0.15λ.

Table 1. Comparison results of FWHM and focusing efficiency.

Focal length (μm)	Quadratic-phase zoom metasurface		Airy zoom metasurface ($\varepsilon = 0.25$)	
	FWHM (nm)	Focusing efficiency	FWHM (nm)	Focusing efficiency
8	568	9%	440	11%
16	736	22%	632	24%
24	1112	24%	880	25%
32	1344	26%	1288	24%

4. Summary

In conclusion, we propose a tunable Airy zoom metasurface based on the moiré effect by integrating the Airy autofocusing phase with a rotational metasurface configuration. The bilayer structure enables continuous control of the Airy beam focal position through relative rotation between the two metasurfaces, providing a compact strategy for dynamic beam manipulation without translational mechanical components. Numerical results confirm that the proposed design maintains the propagation characteristics of Airy beams while improving focusing performance compared to quadratic-phase moiré zoom metasurfaces. Furthermore, the parameter ε, describing the ratio between the inner and outer radii of the metasurface, is shown to strongly influence the focusing behavior and should be optimized according to the system numerical aperture. Future work will focus on experimental realization and extending the concept to broadband and multifunctional tunable metasurface devices.

Acknowledgements

This work was supported by the National Natural Science Foundation of China (Grant No. 62504057) and the Special Fund for Science and Technology Development of Guangxi Zhuang Autonomous Region, China (Grant No. AD25069078).

References

[1] Efremidis N K and Christodoulides D N 2010 *Opt. Lett.* **35** 4045
[2] Papazoglou D G, Efremidis N K, Christodoulides D N and Tzortzakis S 2011 *Opt. Lett.* **36** 1842
[3] Li W, Cheng S, Yi Z, Zhang H, Song Q, Hao Z, Sun T, Wu P, Zeng Q and Raza R 2025 *Appl. Phys. Lett.* **126** 033503
[4] Ai Z, Liu H, Cheng S, Zhang H, Yi Z, Zeng Q, Wu P, Zhang J, Tang C and Hao Z 2025 *J. Phys. D: Appl. Phys.* **58** 185305
[5] Li Z, Cheng S, Zhang H, Yang W, Yi Z, Yi Y, Wang J, Ahmad S and Raza R 2025 *Phys. Lett. A* **534** 130262
[6] Cheng S, Li W, Zhang H, Akhtar M N, Yi Z, Zeng Q, Ma C, Sun T, Wu P and Ahmad S 2024 *Opt. Commun.* **569** 130816
[7] West P R, Stewart J L, Kildishev A V, Shalaev V M, Shkunov V V, Strohkendl F, Zakharenkov Y A, Dodds R K and Byren R 2014 *Opt. Express* **22** 26212

[8] Aieta F, Genevet P, Kats M A, Yu N, Blanchard R, Gaburro Z and Capasso F 2012 *Nano Lett.* **12** 4932

[9] Monticone F, Estakhri N M and Alù A 2013 *Phys. Rev. Lett.* **110** 203903

[10] Fattal D, Li J, Peng Z, Fiorentino M and Beausoleil R G 2010 *Nat. Photonics* **4** 466

[11] Yu N and Capasso F 2014 *Nat. Mater.* **13** 139

[12] Meinzer N, Barnes W L and Hooper I R 2014 *Nat. Photonics* **8** 889

[13] Kildishev A V, Boltasseva A and Shalaev V M 2013 *Science* **339** 1232009

[14] Jahani S and Jacob Z 2016 *Nat. Nanotechnol.* **11** 23

[15] Krasnok A E, Miroshnichenko A E, Belov P A and Kivshar Y S 2012 *Opt. Express* **20** 20599

[16] Lin D, Fan P, Hasman E and Brongersma M L 2014 *Science* **345** 298

[17] Sun S, He Q, Xiao S, Xu Q, Li X and Zhou L 2012 *Nat. Mater.* **11** 426

[18] Qin F, Ding L, Zhang L, Monticone F, Chum C C, Deng J, Mei S, Li Y, Teng J and Hong M 2016 *Sci. Adv.* **2** e1501168

[19] Ding X, Monticone F, Zhang K, Zhang L, Gao D, Burokur S N, De Lustrac A, Wu Q, Qiu C W and Alù A 2015 *Adv. Mater.* **27** 1195

[20] Yu N, Aieta F, Genevet P, Kats M A, Gaburro Z and Capasso F 2012 *Nano Lett.* **12** 6328

[21] Ni X, Kildishev A V and Shalaev V M 2013 *Nat. Commun.* **4** 2807

[22] Liu N N, Tan L, Chen K J, Hong P L, Mo X M, Zou B S, Ren Y X and Liang Y 2024 *Chin. Phys. B* **33** 064201

[23] Liu N N, Tang X Y, Liu S Y and Liang Y 2024 *Chin. Phys. B* **33** 054201

[24] Colburn S, Zhan A and Majumdar A 2018 *Optica* **5** 825

[25] Wei Y, Wang Y, Feng X, Xiao S, Wang Z, Hu T, Hu M, Song J, Wegener M and Zhao M 2020 *Adv. Opt. Mater.* **8** 2000142

[26] Kaminer I, Segev M and Christodoulides D N 2011 *Phys. Rev. Lett.* **106** 213903

[27] Wang X, Chu X and Zhou L 2021 *J. Opt. Soc. Am. A* **39** 1

[28] Devlin R C, Khorasaninejad M, Chen W T, Oh J and Capasso F 2016 *Proc. Natl. Acad. Sci. USA* **113** 10473

[29] Zhou W, Li S, Li Y, Chen Z, Yuan M, Zhao F, Chen Y, Chen H, Zhang Z and Wu J 2025 *Nanophotonics* **14** 5251